



Optimizing dot-in-a-well infrared detector architecture for achieving high optical and device efficiency corroborated with theoretically simulated model

H. Ghadi^a, J. Patwari^b, P. Murkute^c, D. Das^a, P.K. Singh^d, S. Dubey^e, M. Bhatt^f,
A. Chatterjee^b, A. Balgarkashi^a, S.K. Pal^b, S. Chakrabarti^{a,*}

^a Department of Electrical Engineering, Indian Institute of Technology Bombay, Maharashtra, 400076, India

^b Department of Chemical, Biological and Macromolecular Sciences, S N Bose National Centre for Basic Sciences, Kolkata, 700106, India

^c Centre for Research in Nanotechnology and Science, Indian Institute of Technology Bombay, Maharashtra, 400076, India

^d Department of Electrical Engineering, Indian Institute of Technology Roorkee, Uttarakhand, 247667, India

^e Department of Electrical Engineering, Malaviya National Institute of Technology, Jaipur, Rajasthan, 302017, India

^f Department of Electrical Engineering, Sardar Vallabhbhai National Institute of Technology, Gujarat, 395007, India

ARTICLE INFO

Article history:

Received 23 January 2018

Accepted 1 April 2018

Available online 4 April 2018

Keywords:

Quantum dots

Strain reducing ternary alloy

Photoluminescence

Time resolved photoluminescence

Spectral response

Photodetectors and infrared detectors

ABSTRACT

Dot-in-a-well (DWELL) heterostructures have been extensively researched in quantum dot based infrared photo-detectors as it offers tuning of detection peak wavelength, low dark current and a higher operating temperature with optimized quantum well thickness. In this paper, we have correlated experimentally observed opto-electronic properties of three different InAs quantum dots in DWELL configuration with varying ternary capping ($\text{In}_{0.15}\text{Ga}_{0.85}\text{As}$ - Strain reducing ternary alloy) thickness from 4 to 8 nm to the proposed simulation model for achieving high efficiency in device performance. Low temperature (8 K) photoluminescence (PL) spectra exhibits a blue shift of around 24 nm along with a decrease in intensity as the capping thickness increases above 6 nm. Decrease in full width at half maximum (FWHM) value for PL peak was observed as the capping thickness is increased from 6 to 8 nm. These are attributed to formation of InGaAs quantum wells via dots sublimation process. Presence of InGaAs wells for 8 nm capped sample was confirmed using low temperature photoluminescence measurement at 2.54 W/cm^2 and photoluminescence excitation (PLE). Time resolved photoluminescence spectroscopy gave further insight into the carrier dynamics of the grown structures and confirms undesirable quantum well formation in 8 nm capped sample. Improved optical characteristics with formation of defect-free structure having larger quantum dot was achieved in 6 nm capped sample affirmed using transmission electron microscopy images. Low dark current density with high confinement energy was achieved from 6 nm capped DWELL structure. Dominant spectral response peak was obtained at $7.56 \mu\text{m}$ from all the samples. A concentration-dependent theoretical strain model using the Schrödinger equation was developed to calculate the potential, ground-state and inter-sub band energy-levels. It was validated by comparing experimentally achieved PL and PLE peaks along with spectral response peaks. The theoretical model was used to calculate the energy levels corresponding to conduction and valence bands for InGaAs well and indium concentration in the well was obtained to be around 30%. Similarly, concentration dependent 2D to 3D transition for $\text{In}_x\text{Ga}_{1-x}\text{As}$ ($0 \leq x \leq 1$) quantum dots formation was modelled using People-Bean relation which matches with the proposed simulation.

© 2018 Elsevier B.V. All rights reserved.

1. Introduction

Self-assembled InAs/GaAs quantum dots (QDs) have received

considerable attention, due to their promising applications in opto-electronic devices [1–5]. The development of the InAs/GaAs QD based optical devices has progressed rapidly. However, the performance of such optical devices is still not satisfactory, due to their inability to tune the emission wavelength to certain desired values (3–5 and 8–14 μm) which are suitable for optical fiber communication systems and infrared detectors. Hence, the dots-in-a-well

* Corresponding author.

E-mail address: subho@ee.iitb.ac.in (S. Chakrabarti).

(DWELL) structure has been widely investigated in the last decade as they provide tunability of emission wavelength [6–8]. InAs quantum dots are enclosed in asymmetric InGaAs wells and further capped with a GaAs barrier in a DWELL configuration. This DWELL design is based on optical transitions between dot and quantum well (QW) states and offers additional possibility to vary transition energy by adjusting QW width and composition. To optimize the operation of such devices it is essential to know their optical properties and electronic structures in detail [9] Quantum Dot Infrared Photodetectors (QDIPs) fabricated from DWELL are used to study the device properties as they offer low dark current and higher operating temperature with optimized quantum well thickness, thus increasing the quantum efficiency.

For DWELL structures the emission wavelength can be tuned by varying InGaAs strain-reducing layer (SRL) capping thickness. It causes the relaxation of the compressive strain around the QDs and In-Ga intermixing between the capping layer and the QDs is suppressed [9–11]. Also, the morphology and emission wavelength can be varied by changing the InGaAs strained buffer layer (SBL) or pseudo-morphic layer [10–13]. Thus, in DWELL structures, growth parameters for the well layer, such as thickness and composition of the SBL and SRL, can be tuned to match the wavelength. While considerable efforts have been made to study the effect of composition of capping layer on the optical properties of the DWELL structure [14–16], very few studies have explored the effect of variation of the well thickness on its optical and electronic properties. It's a conventional approach to introduce ternary or quaternary capping over QDs to reduce interdiffusion and provide an additional energy level for inter-subband transition. Even though it is beneficial, these capping thickness and molar concentration have to be optimized. Almost every report in literature suggests increasing capping layer thickness benefits in QD formation and improves device performance [10–16]. A detailed analysis i.e. photo physics, structural, device characterization and correlation with theoretical simulation is yet to be reported. A higher quantum and optical efficiency can be obtained by changing the well thickness and deducing an optimized DWELL configuration.

In this report, we have studied the effect of variation of well thickness in three samples of InAs/InGaAs DWELL structure. The strain reducing layer is varied (viz. 4, 6 and 8 nm) keeping the pseudo-morphic layer fixed. The optical and device properties of three samples are compared. A concentration dependent strain model is developed to correlate our experimental results with the simulated results. The energy transitions obtained in the experimental model are compared with the peaks in the spectral

response and thus the model is validated. This report is a detail study on DWELL systems by emphasizing on optical (Photoluminescence & Time resolved Photoluminescence), structural (Transmission electron microscopy) and simulated results to establish a good correlation with the fabricated device characteristics.

2. Experimental methods

2.1. Growth of samples

The samples were grown using solid state Molecular Beam Epitaxy method (MBE) with Stranski Krastanov being the growth mode. The three samples consist of the active layer of 10 layers of quantum dots with a subsequent capping/barrier. A 1000 nm n-type GaAs layer grown at 590 °C followed by intrinsic GaAs layer of 217 nm is deposited before active layer. In active region of all three samples, the bottom $\text{In}_{0.15}\text{Ga}_{0.85}\text{As}$ layer (Pseudomorphic layer) thickness is kept constant at 2 nm. The upper capping layer ($\text{In}_{0.15}\text{Ga}_{0.85}\text{As}$ – Strain reducing layer) thickness is varied by 4, 6 and 8 nm in samples A, B and C, respectively. In all samples 2.7 monolayer (ML) of InAs quantum dots were deposited at 490 °C and the whole active region was finally capped with 50 nm GaAs barrier to avoid coupling. A top n-type contact layer of 200 nm was deposited at 490 °C. Fig. 1 depicts DWELL heterostructure used in our study. The active region of the three samples was grown at 500 °C. The growth rate was kept same for all. Table 1 shows the parameters which were varied in the different heterostructures.

2.2. Measurement details

Photoluminescence measurements at 8–300 K were performed for all the samples in order to determine their optical characteristics. Helium flow controlled closed cycle cryostat was used to perform PL measurements. The mounted samples were excited with a green continuous wave laser of wavelength 532 nm and variable laser power. A high pass filter (645 nm) was used to pass only specific range of wavelength. A liquid nitrogen cooled InGaAs array detector was used to detect the emitted luminescence signal along the normal direction. This signal was obtained after dispersion by a 600 g/mm grating in a 750 mm focal length spectrometer. In Photoluminescence excitation spectroscopy, emission wavelength is fixed to ground state achieved from PL spectrum and the excitation wavelength is varied to observe higher energy peak from single dot. Halogen lamp as a light source was used for irradiating

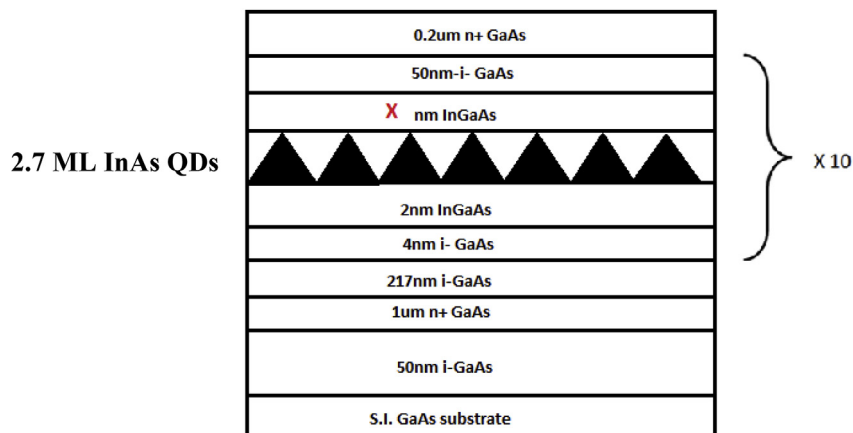


Fig. 1. Schematic diagram of DWELL samples A, B and C.

Table 1
Capping layer variation for three samples.

Sample	X
A	4
B	6
C	8

sample kept in He-closed cycle cryostat (8–300 K). The incident light was dispersed through 0.75 nm monochromator and the obtained PLE signal was sampled using chopper and lock in amplifier (to reduce noise). This signal was through a 0.75 nm monochromator and collected in InGaAs detector. The input side monochromator grating was fixed at 600 g/mm and output side to 300 g/mm.

The picosecond time resolved photoluminescence (TRPL) transients have been measured by a custom made time correlated single photon counting (TCSPC) setup. Picosecond pulsed lasers of Pico-quant (510 nm wavelength) has been used as excitation source in this study. The instrument response function was measured to be 200 ps. The excited state lifetimes were calculated by fitting the PL decays in Scientist software. High resolution images were measured using FEI made Tecnai G2, F30 model high resolution transmission electron microscopy.

2.3. Device characterization

A standard two level lithography process was utilized and the detector fabrication process is reported in our earlier published studies [1,17–19] A Thermo Fisher Fourier transform infrared spectrometer was used for measuring the spectral response in which the fabricated devices were fixed and wire-bonded onto a 64-pin leadless chip carrier and mounted on a liquid nitrogen pour fill cryostat. A cold radiation shield was fitted in the cryostat for dark current and noise measurements. Temperature-dependent voltage vs. dark current, noise and spectral response were measured.

2.4. Theoretical modelling [17–19]

2.4.1. InAs/InGaAs quantum dots parametric equations

A concentration dependent strain model is developed to simulate the InAs/InGaAs Dwell structure. The different parameters of InGaAs depend on the concentration of In (c) and are depicted as follows-

$$\left. \begin{aligned} E_g &= 0.475c^2 - 1.575c + 1.52 \\ m_e &= 0.04c + 0.665(1 - c) \end{aligned} \right\} \quad (1)$$

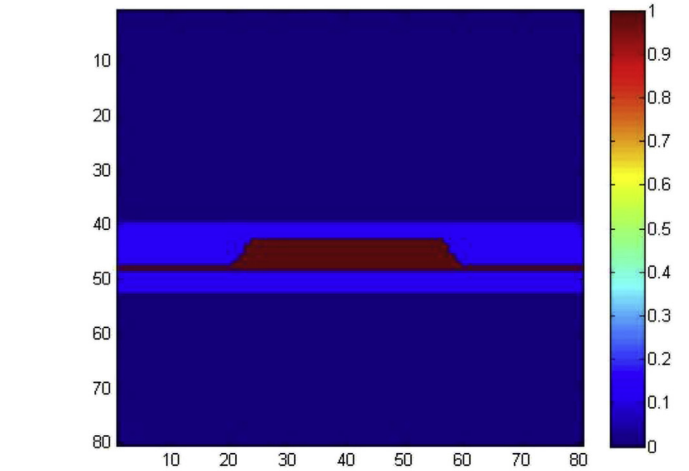
As shown in Fig. 2(a), QDs are considered to be of truncated pyramidal structure. The dimensions for InAs QDs are considered from TEM images. The effect of increasing the capping thickness of In_{0.15}Ga_{0.85}As on the transition energies is studied. The observed conduction band profile are shown in Fig. 2(b).

2.4.2. Strain equations [17,18]

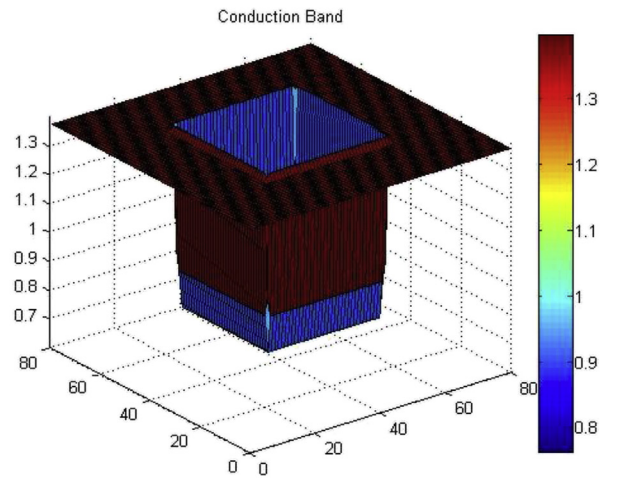
The methodology for the calculation of strain and energy levels remains the same, irrespective of capping. We calculate strain using equation (2).

$$\epsilon = \frac{a_x - a_0}{a_0} \quad (2)$$

Here, a_x and a₀ represent the lattice constant of the epitaxial layer and substrate, respectively. The various parameters used in the



(a)



(b)

Fig. 2. (a). Simulated truncated pyramidal structure for sample B. (b). Conduction band diagram achieved for sample B.

strain model are concentration dependent and are calculated from equations (3)–(6),

The elastic coefficient is calculated as follows [10]:

$$\left. \begin{aligned} c_{11} &= (12.23 - 3.9c_{in}) * 10^{11} \text{ dynes/cm}^2 \\ c_{12} &= (5.71 - 1.18c_{in}) * 10^{11} \text{ dynes/cm}^2 \end{aligned} \right\} \quad (3)$$

The hydrostatic pressure coefficient is expressed as follows: 10

$$\frac{dE_g}{dP} = (11.3 - 1.1c_{in}) eV/bal \quad (4)$$

The effect on the confinement caused by the hydrostatic component of strain can be expressed as follows:

$$S_{\perp} = -2a \left(1 - \frac{c_{12}}{c_{11}} \right) \epsilon \quad (5)$$

Here, “a” is the hydrostatic deformation potential expressed as follows:

$$a = -\frac{1}{3} (c_{11} + 2c_{12}) \frac{dE_g}{dP} \quad (6)$$

The conduction band (CB) offset and valence band (VB) offset using Andersons rule is in a 66/34 ratio for InGaAs.

Strain potential is obtained from equation (7).

$$V = \Delta E * S_{\perp} \quad (7)$$

Here, ΔE is the offset in the respective bands.

2.4.3. Energy state equations [17,18]

Schrödinger's equation (8) was employed to calculate energy levels of the heterostructure for both electrons and holes.

$$H\psi = -\frac{\hbar^2}{2} \nabla \cdot \left(\frac{1}{m^*} \nabla \psi \right) + V\psi = E\psi \quad (8)$$

The finite-difference approximation has been used with the Dirichlet boundary conditions imposed on the wavefunction, resulting in an eigenvalue problem, where the Hamiltonian is the matrix formed by the calculations presented before, and energies are obtained as its eigenvalues. The potential described in the Schrodinger equation above accounts only the lattice formed potential; however, to handle electronic interaction among carriers, we need to solve the Poisson equation (9).

$$\nabla^2 V = \frac{\rho}{\epsilon} \quad (9)$$

Linear interpolation of permittivity is possible using Vegard's law and the electrostatic energy was calculated using equation (10).

$$E_{coul} = \int \rho V d\tau \quad (10)$$

All the calculated energies are added and the photoluminescence E_{PL} energy peak obtained is as follows (equation (11)):

$$E_{PL} = E_{coul} + E_{conf}^e + E_{conf}^h \quad (11)$$

Here, E_{conf}^e and E_{conf}^h represent the electron and hole confinement energies, respectively.

In the simulation, we have defined band gap as the separation between the bottom CB to the top of VB (heavy hole branch). Strain causes deviation in the potential values of energy levels as it acts as a perturbation and hence lifts the degeneracy among the light and heavy holes. The band gap decreases as the heavy hole branch moves up keeping the conduction band minima to be fixed. As a result of the spatial variation in strain strength in the sample, this band gap decrease is detectable at the edges as strain attains its maximum. In other words, the greater the strain, the lesser is the band gap. Hence, at low temperature, strain is considerably strong, band gap reduces; hence, CB exhibits a dip at the edges [17–19].

2.4.4. InGaAs quantum well simulation

As the capping thickness is increased beyond 6 nm, the dissolution of dots predominates leading to the formation of InGaAs well. The well is formed with a concentration gradient of In from the center (InAs dots, In-100%) to the periphery (In-15%) of the capping layer. The theoretical model was modified to compute the energy band of the InGaAs Well with varying In concentration. The experimental data was compared with the theoretical model and the percentage of In in the InGaAs well was calculated. For the theoretical model the average In concentration in the well is calculated instead of the concentration gradient in the well.

In this model, we use the finite difference method for calculating the Hamiltonian matrix and the corresponding Eigen values while taking into account the effective mass differences at the interface.

We discretize the position variable x into a lattice of points such that the spacing between the points is equal to a . The representation becomes exact only in the limit $a \rightarrow 0$ but as long as 'a' is smaller than the spatial scale on which ψ varies, it is expected to be reasonably accurate.

The thickness of the InGaAs wells formed is considered to be 6 nm for sample A, 8 nm for sample B and 10 nm for sample C including the 2 nm pseudo-morphic InGaAs layer below the dot layer. Same parametric equations as InAs QDs are used in InGaAs well.

3. Results and discussion

3.1. Optical characterization

3.1.1. Photoluminescence

Low temperature (8 K) photoluminescence (PL) spectrum exhibits maximum peak intensity at 1142.74, 1166.93 and 1140.38 nm for the samples A, B and C, respectively as shown in Fig. 3. A threefold increase in highest peak intensity was measured from sample B at 8 K. A red shift obtained in sample B can be attributed to formation of larger dots (increase in height of QD) with increase in capping layer thickness. This is due to reduction in the compressive strain on the quantum dots layer which results in better vertical confinement [10–12] Blue shift of around 24 nm with a decrease in intensity was obtained when the capping thickness was further increased from 6 to 8 nm. This is attributed to reduction in surface migration process with increasing strain reducing layer thickness. As the capping thickness increases another dominant process to hinder the growth is low surface transport of indium atoms. Reduced surface migration process leads to formation of QD in two possible scenarios. Firstly, the growth in vertical direction is restricted resulting in bigger dots with smaller height i.e. dots are laterally stretched and vertically squeezed. In second scenario, smaller InAs dots coalesce with one another and dissolve, giving rise to formation of InGaAs well with varying In concentration.

For highest capping thickness, InAs dot layer between the strain reducing layer (SRL) and the pseudomorphic layer (bottom 2 nm InGaAs layer) dissolves thus forming InGaAs wells with non-linear In concentration. Consequently, the concentration of In gradually decreases from the center of the well to the edges. Subsidiary peaks obtained at 1080.86, 1104.84 and 1085.02 nm for samples A, B and

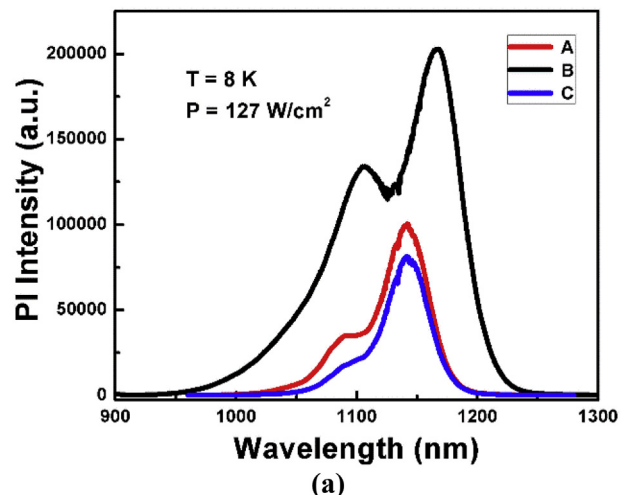


Fig. 3. Photoluminescence intensity measured at 8 K. Power density 127 W/cm².

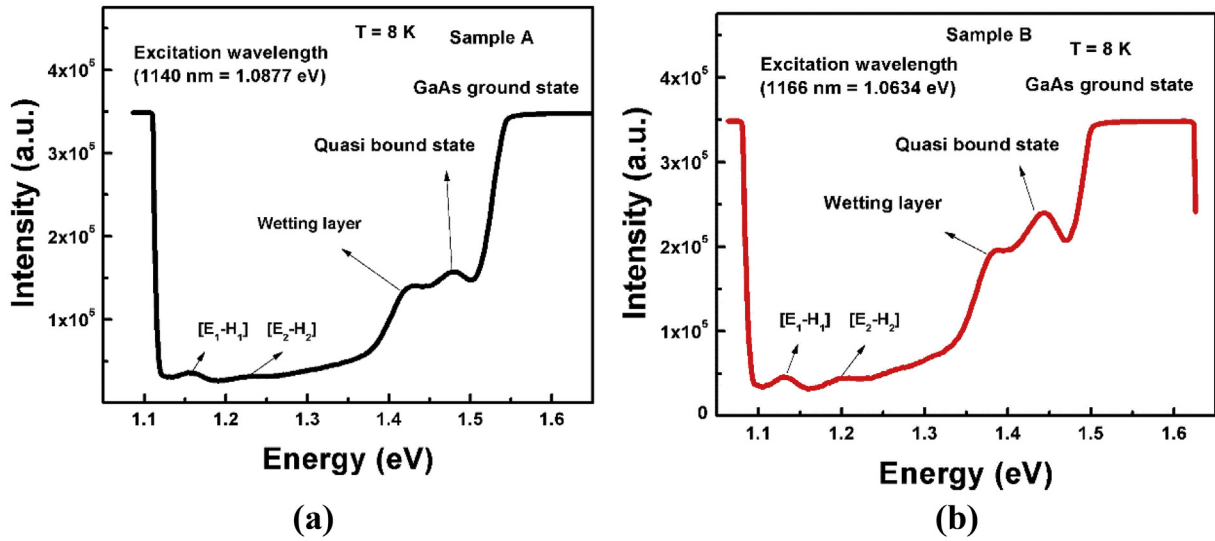


Fig. 4. PLE Spectra measured at 8 K (a) for ground state peak at 1140 nm in sample A (b) for ground state peak at 1166 nm in sample B.

C, respectively (Fig. 3) were the ground state peaks of the InGaAs well structure.

Maximum absolute area was achieved from sample B. Also, the FWHM is the maximum for sample B. An increase in FWHM suggests non-uniform dot size distribution. The FWHM further decreases for sample C due to the dissolution of the quantum dots. In sample B, even though there is non-uniformity in QD size distribution a significantly high PL intensity was observed. Increase in intensity is achieved possibly because of increasing density of dots available for absorption. The SRL layer provides In gradient across the dot to reduce out-diffusion and also act as a strain reducing layer thus forming bigger dots. For thin capped samples, strain relaxation and out-diffusion process are limited whereas increasing capping layer above an optimum thickness might result in dots sublimation. Hence, above a particular capping thickness (6 nm) a reduction in PL intensity with blue shift is observed [17–22].

Temperature dependent PL measurement was carried out and thermal escape energy was calculated using standard process reported in our earlier work [17–19]. Sample B exhibited highest thermal escape energy in comparison with others. The achieved

activation energies for sample A, B and C were 201.46, 232.96 and 193.65 meV, respectively. High activation energy suggests better confinement with a possibility of improved device performance.

3.1.2. Photoluminescence excitation

The photoluminescence excitation (PLE) spectra for all samples are shown in Figs. 4 and 5. PLE measurement indicates the presence of first and second excited state at 1074.62 and 1006.11 nm for sample A (Fig. 4 (a)), 1098.55 and 1034.51 nm for sample B (Fig. 4 (b)) and 1062.98 and 1003.34 nm for sample C (Fig. 5 (a)). The observed first excited state values in sample A and B are within the range whereas in case of sample C the transition appeared to be from some other confinement.

To further investigate PLE spectra, keeping the emission wavelength fixed at 1085.02 nm for sample C measured first excited state peak was at 981.4 (1.2635 eV) nm and second excited state at 879.3 (1.412 eV), respectively. The PLE signature for Fig. 5 (b) is different from ground state PLE spectrum measured from (Fig. 5 (a)). Hence it can be deduced here that owing to the dissolution of dots, there exists a gradient of In concentration in the space between two

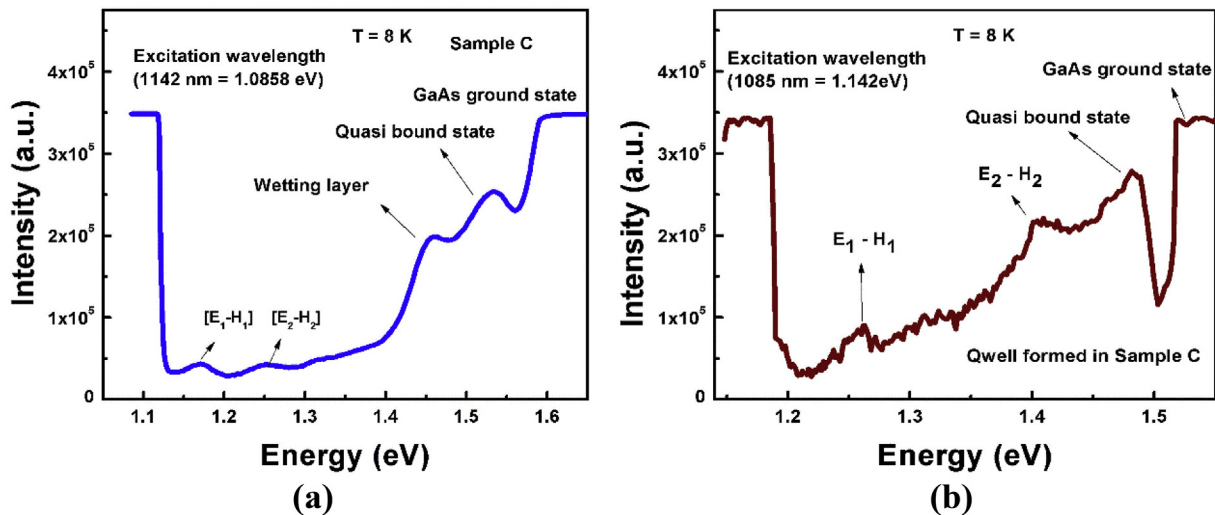


Fig. 5. (a) 8 K PLE spectra measured at 1142 nm (ground state) from Sample C (b) 8 K PLE spectra from probable InGaAs well formed at 1085 nm in sample C.

InGaAs layers (SRL and Pseudomorphic layer) forming a new confined structure. Increasing capping thickness arises the possibility of InGaAs quantum well formation thus lowering device performance in DWELL structures. The PLE spectra measured at lower wavelength for samples A and B exhibited a blue shift having similar response as shown in Fig. 5(a) and (b) indicating the origin of spectrum from same source i.e. quantum dots.

3.1.3. Time resolved photoluminescence spectroscopy

It is evident from Fig. 6 that the excited state PL decay lifetimes from the measured PL peaks (ground and excited states) are the signature of radiative recombination at different energy levels. The higher energy hump of the PL is associated with a radiative recombination within the capping layer where the excited state lifetime has one rise component and one decay component. As, the TRPL has been measured upon a non-resonant high energy excitation, the rise component of 220 ps can be assigned to the carrier migration timescale from barrier GaAs to the capping layer InGaAs while the radiative decay lifetime is 0.81 ns and 1 ns respectively for the 4 nm and 6 nm capping layer samples at 80 K temperature. The red-shifted higher intensity PL peak is most likely due to the ground state recombination (e_0-h_0) within the InAs QD having

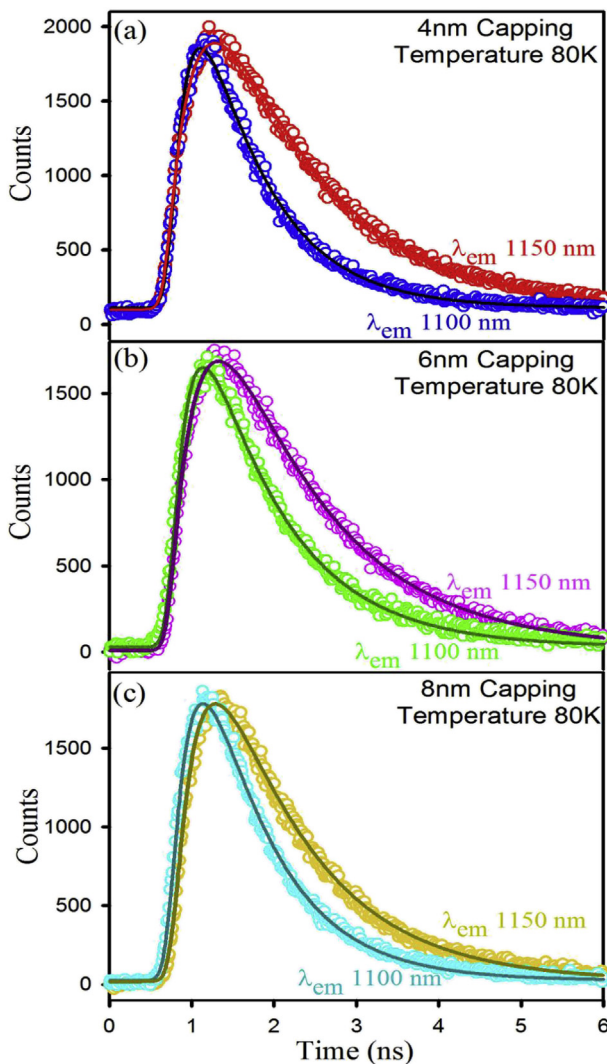


Fig. 6. Pico-second resolved photoluminescence transients of (a) 4 nm capping, (b) 6 nm capping, (c) 8 nm capping DWELL samples at different PL peak positions.

Table 2

Excited state lifetimes from the fitting details of TRPL data for sample A.

Emission Wavelength (nm)	Temperature (K)	τ_1 (ns) Rise Component	τ_2 (ns) Decay Component	τ_3 (ns) Decay Component
1100	80	0.22 (50%)	0.81 (50%)	
1100	100	0.22 (49%)	0.85 (51%)	
1100	120	0.27 (50%)	0.85 (50%)	
1100	140	0.27 (50%)	0.85 (50%)	
1150	80	0.35 (46%)	1.52 (24%)	1.1 (30%)
1150	100	0.35 (47%)	1.97 (20%)	1.2 (33%)
1150	120	0.35 (46%)	2.18 (16%)	1.4 (38%)
1150	140	0.35 (47%)	2.67 (18%)	1.2 (34%)

Table 3

Excited state lifetimes from the fitting details of TRPL data for sample B.

Emission Wavelength (nm)	Temperature (K)	τ_1 (ns) Rise Component	τ_2 (ns) Decay Component	τ_3 (ns) Decay Component
1100	80	0.22 (50%)	1.00 (50%)	
1100	100	0.24 (50%)	1.00 (50%)	
1170	80	0.27 (50%)	1.36 (16%)	1.00 (34%)
1170	100	0.35 (52%)	1.63 (21%)	1.00 (27%)

three components of lifetimes in both the cases of 4 nm capping (Table 2) and 6 nm capping (Table 3). The rise component at this state is higher in time scale i.e. 350 ps due to the carrier migration both from the GaAs barrier and the InGaAs capping layer. There have been two decay timescales associated with the excited state of the InAs QDs both in case of 4 nm and 6 nm samples. The longer one is the radiative recombination timescale and the shorter decay timescale can be ascribed to the non-radiative carrier loss mechanisms. The 8 nm capping (Table 4) sample is showing a different decay pattern with two exponential time scales at the 1150 nm PL peak position which is an additional proof of suppression of vertical growth of InAs QDs with increasing capping layer thickness and decreased QD confinement (or dissolved dots). Comparing the decay patterns for three of the samples it can be concluded that with increasing capping layer thickness the carrier lifetimes at InAs QD are behaving similar. For the 8 nm samples, both the carrier lifetimes at ground and excited states are having single rise and single decay pattern unlike the other two samples.

Fig. 7 shows the temperature dependent nature of the PL transients, where it can be observed that for the 4 nm sample the excited state peak position is not much affected by temperature while for ground state peak the radiative recombination timescale is gradually increasing with the increase in temperature [23,24]. This particular observation is consistent with earlier reported

Table 4

Excited state lifetimes from the fitting details of TRPL data for sample C.

Emission Wavelength (nm)	Temperature (K)	τ_1 (ns) Rise Component	τ_2 (ns) Decay Component	τ_3 (ns) Decay Component
1100	80	0.24 (50%)	0.84 (43%)	0.48 (7%)
1100	100	0.25 (49%)	0.84 (51%)	
1100	120	0.25 (50%)	0.97 (50%)	
1100	140	0.25 (50%)	1.27 (50%)	
1100	160	0.25 (50%)	1.15 (50%)	
1150	80	0.28 (50%)	1.2 (50%)	
1150	100	0.35 (47%)	1.4 (53%)	
1150	120	0.35 (46%)	1.5 (54%)	
1150	140	0.35 (45%)	1.6 (55%)	
1150	160	0.35 (44%)	1.6 (56%)	

literature [25,26]. The probable reasons behind it is large carrier lifetime of the migrated electrons from barriers and capping layer to the QDs and thermally induced population of dark excitations. In case of the 8 nm sample, the carrier lifetimes at both the peak positions (ground state and other confined Qwell state) are found to be affected by temperature [27] and the overall carrier lifetime has increased with increasing temperature. Lesser QD confinement (or dot sublimation) to some extent leads to the similarity in behaviour of the PL transients at both the peak positions in case of the 8 nm capping sample unlike that with 4 nm which is in good agreement with the conclusions from other studies.

3.2. Transmission electron microscopy (TEM) analysis

Lattice mismatch induced self-assembly in formation of InAs quantum dots over GaAs substrate leads to randomly configured dots having non uniform size distribution. Lack of controllability on the shape and density of formed QDs is evident from Fig. 8.a. All the grown structures were free from defect and dislocation. The pseudo-morphic ternary capping of 2 nm grown underneath of QDs has same lattice constant as that of GaAs. Addition of pseudomorphic layer not only provides an additional energy level but also reduces indium out-diffusion. High resolution TEM images of samples A, B and C are shown in Fig. 8b, c and d, respectively. Increasing SRL capping thickness resulted in monotonic increase in lateral dimension of QD whereas the height of QD decreases. The measured dimensions are tabulated in Table 5 and further used for

simulation.

The critical thickness for forming InAs QD reported in literatures is 1.7 ML. Similarly, for $\text{In}_{0.5}\text{Ga}_{0.5}\text{As}$ QD is 5.1 ML. Using the known experimental values, People-Bean model can be implemented and theoretically indium concentration versus critical thickness for forming InAs QDs can be calculated. The reduced form of equation (12) is [28]:

$$h_c = \frac{(1-\gamma)}{(1+\gamma)} \frac{1}{16\pi\sqrt{2}} \frac{b^2}{a(x)} \left(\frac{1}{f^2}\right) \left(\ln \frac{h_c}{b}\right) \quad (12)$$

Here h_c is critical thickness, γ is Poisson's ratio, b is burgers vector (4.3 nm), $a(x)$ lattice constant of ternary alloy calculated using vegard's law, f is lattice mismatch i.e. ratio of difference of lattice constants of alloy and GaAs to lattice constant of GaAs. From equation no. 12, a plot for critical thickness in monolayer versus indium concentration is depicted in Fig. 9.

Ternary alloys reduces In-Ga interdiffusion thus increasing the dot dimensions. But above a certain capping thickness there is a possibility of forming $\text{In}_x\text{Ga}_{1-x}\text{As}$ dots. For sample C, the total capping thickness including the pseudomorphic layer (i.e. total thickness 8 nm + 2 nm) and sublimation of smaller dots increases the possibility of InGaAs dot formation. Assuming 30% of indium (subsequently, this value we will confirm from theoretical simulation) to be present in the Qwell structure formed, the calculated critical thickness in monolayer using People-Bean model is 41.37 ML (i.e. ~11.94 nm) Since, the indium concentration is non-

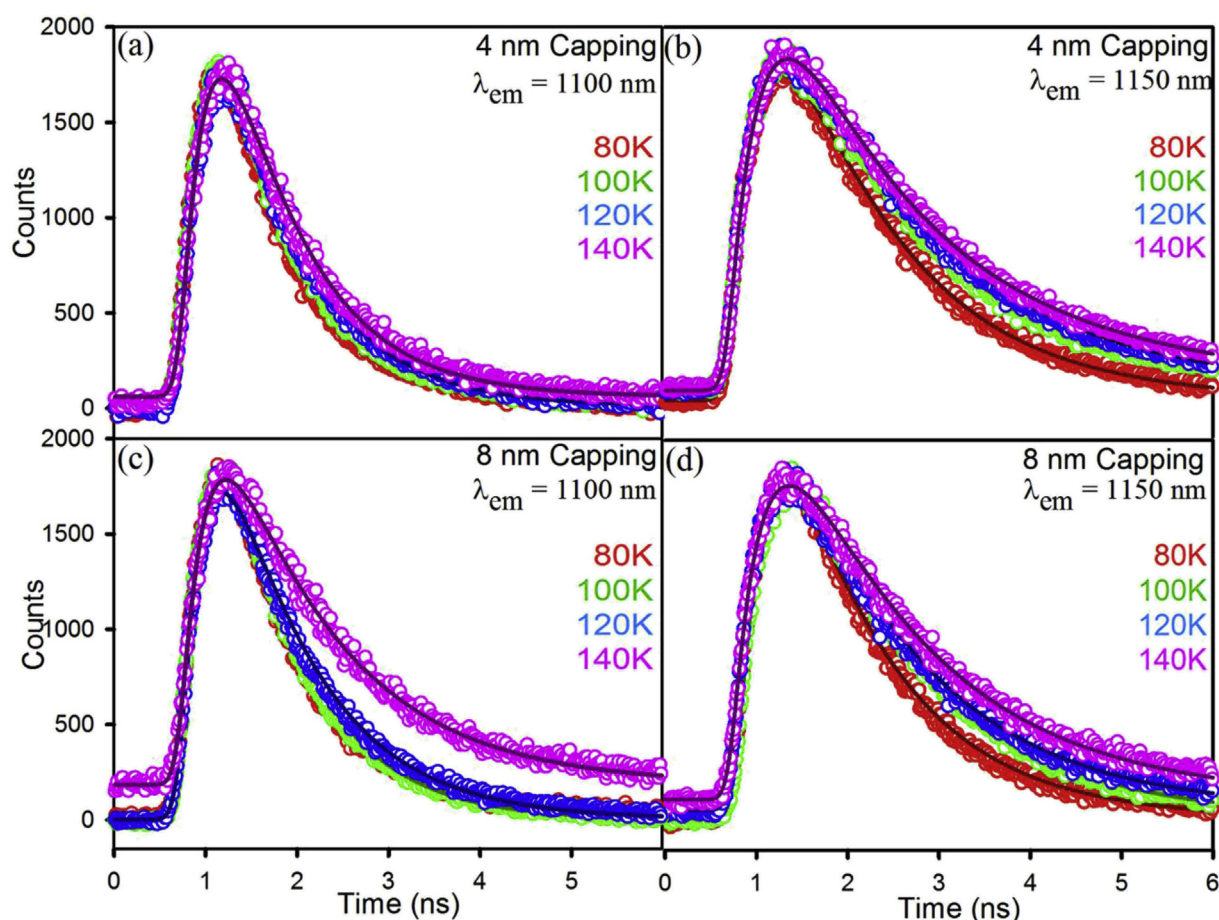


Fig. 7. Temperature dependent time resolved photoluminescence decay profiles of 4 nm Capping and 8 nm Capping DWELL samples at different emission wavelengths.

uniform between the formed layer and the total thickness is near to the critical thickness (i.e. required for 2D to 3D transition) the 3D transition is withheld. So, instead of forming an InGaAs dot a simultaneous InGaAs well is formed between the two GaAs interface. From low resolution TEM image of sample C in Fig. 8.e, it is visible that the lateral spacing between to two QD in the same layer is minimum compared to other samples. It appears to be more like a Qwell structure.

3.3. Device characterization

Single pixel detectors were fabricated and characterized. Dark current is an important parameter to judge detector performance. High temperature of operation and excellent figure of merits (i.e. high detectivity, low dark current density) are essential features of infrared detectors. Minimum dark current density was observed from sample B (Fig. 10). The dominant sources of dark current are thermionic emission and field assisted tunnelling. Another method

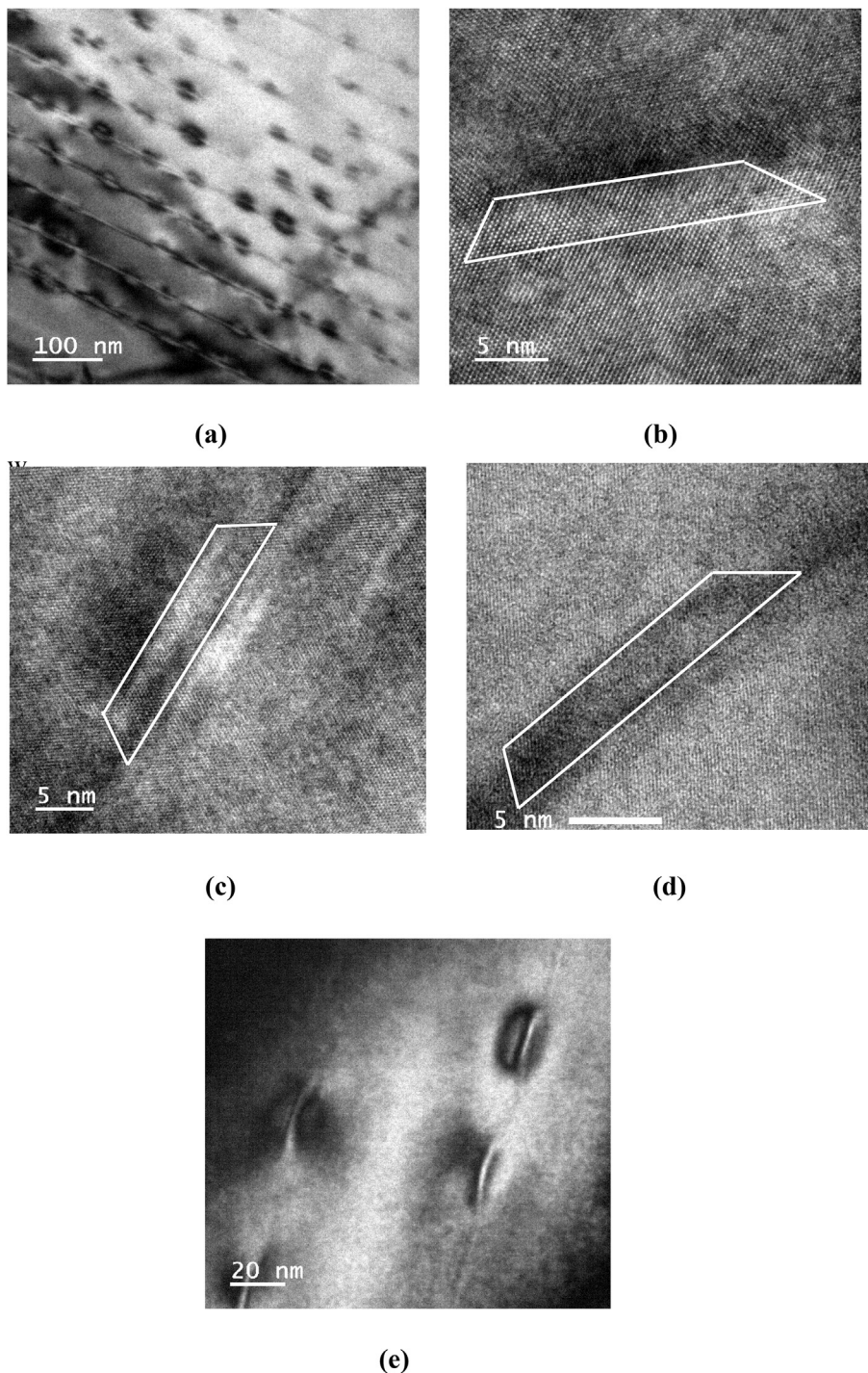


Fig. 8. (a) TEM image of sample A exhibiting all 10 layers. High resolution TEM images of single QD in (b) sample A, (c) sample B, (d) sample C and (e) Two layer TEM image of sample C exhibiting lateral stretching in horizontal direction.

Table 5
Average quantum dot dimension for different samples.

Sample	Base (a2) (nm)	Top (a1) (nm)	Height (h) (nm)
A (4 nm)	23.82	16.51	3.9
B (6 nm)	25.88	20.66	3.5
C (8 nm)	28.92	22.23	2.9

to calculate thermal escape energy is from temperature dependent current voltage characteristics. The current density as a function of various parameters are specified in equation [29]:

$$J_d = 2e\mu F \left(\frac{m^* kT}{2\pi\hbar^2} \right)^{1.5} \left(\left(1 + \left(\frac{\mu F}{v_s} \right)^2 \right)^{-0.5} \left(e^{\frac{E_0 - \beta F}{kT}} \right) \right) \quad (13)$$

Here J_d is the current density at different temperatures T , μ mobility of electron, m^* effective mass of electron, v_s saturation velocity, k & \hbar are Boltzmann and reduced Planck's constant, F electric field, e charge of electron, β fitting parameter and E_0 is the thermal escape energy. β , μ and v_s are calculated by fitting the equation with varying electric field and temperature. For sample B, the calculated values of various fitting parameters β , μ and v_s were 2.89×10^{-27} mC, 3965.24 cm²/V and 2.365×10^4 cm/s. The calculated values for other samples were slightly different ($\pm 10\%$) as compared to sample B but are similar to values reported in literatures. Based on the equation the measured thermal escape energy using current voltage characteristics for A, B and C were 210.69, 241.62 and 198.26 meV for sample A, B and C, respectively. Improved performance is attributed to enhanced optical properties in optimized capping thickness of 6 nm.

Similarly, other photodetectors figure of merits can be extracted by experimental results using specified equations given by S. Wolde et al. Sample B exhibited maximum photoconductive gain (1.86) and highest electron capture probability (0.7) [29]. Higher photoconductive gain and better capture probability affirms improvement in device performance with optimized capping thickness (6 nm). Responsivity and detectivity are important figure of merits for an Infrared detector. High detectivity is essential for better device performance. Peak responsivity and detectivity calculation details are reported in our earlier work [1]. The measured values of

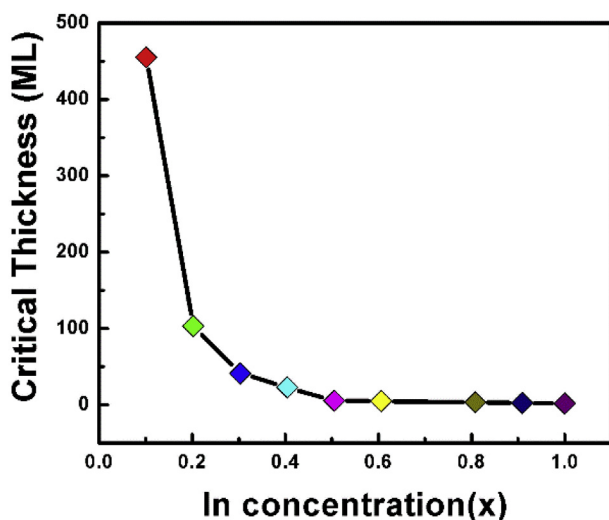


Fig. 9. Critical thickness as a function of indium concentration from People-Bean relation.

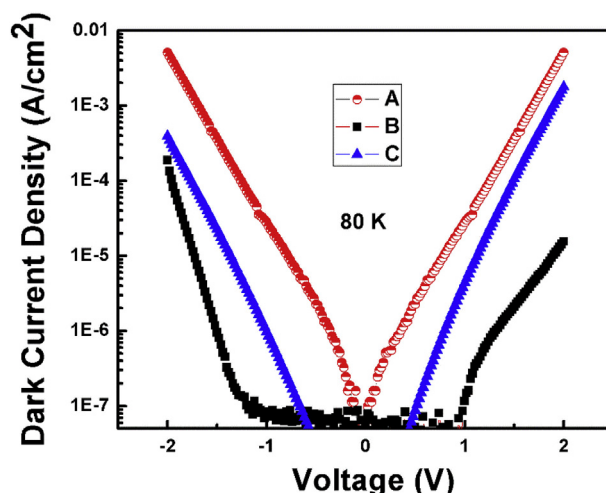


Fig. 10. Dark current density as function of applied bias at 80 K.

responsivity at 80 K were 0.12, 0.33 and 0.075 A/W for samples A, B and C, respectively. Highest detectivity of 7.89×10^8 jones was measured from optimized sample B.

The energy band diagram of InAs/InGaAs Dwell structure was obtained for samples A, B and C by simulating the theoretical model [17–19]. Fig. 11 represents the simulated energy levels for sample B. Specific transitions are highlighted in the band diagram.

The simulated thermal escape energies values for sample A, B and C were 203.2, 251.63 and 195.67 meV. The values are comparable to the experimentally calculated energies. The Energy level calculated for first three transitions and other important transitions are tabulated in Table 6. The decrement in the difference of the energy levels of the excited states as the order of transition increases ratifies the preciseness of the model and provides us with energy of the ground and higher excited states. The energy difference increases as the confinement reduces. The energy difference in sample C drastically increases as we consider higher energy level, phenomena exhibited by smaller dots. As the dot is laterally stretched and vertically suppressed it essentially affects the higher energy levels since the waveform overlap will be minimum.

Figs. 12–14 shows the comparison of spectral response with the inter sub band energies obtained from the theoretical simulation. The different transitions have been highlighted. Spectral response peaks are comparable to the energy levels calculated from the simulation. The peak spectral response of all the samples was $7.56 \mu\text{m}$. The spectral response signal is Fourier transform of all the possible transitions happening in conduction band for different sizes of QDs. The cumulative signal or the various optical results can be achieved by varying the input dot size in the proposed simulation. A dominant spectral response peak at $7.6 \mu\text{m}$ was obtained from sample A and B whereas in case of sample C the peak value was shifted to $7.5 \mu\text{m}$. Formation of bigger dots with higher confinement resulted in increased intensity or photocurrent in sample B whereas it decreases in sample C which is primarily due to formation of Qwell resulting in low absorption of normal incident light. A similar result i.e. decrease in responsivity and detectivity was observed from sample B to C.

All samples exhibited high photocurrent at reasonably high operating temperature of 90 K. Optimized sample B exhibited spectral response upto 100 K and blackbody signal lasting till 140 K. High temperature of operability with improved device performance was achieved in sample B with optimized capping thickness

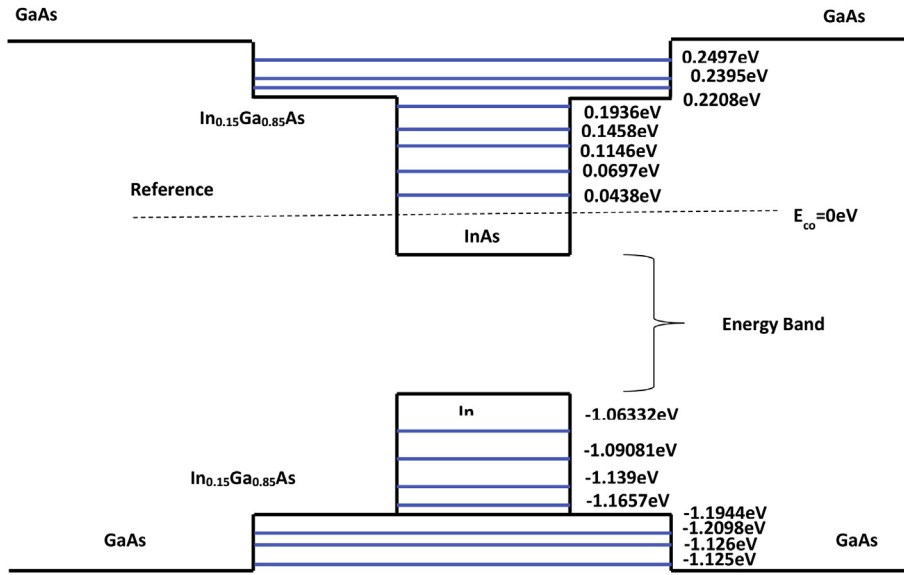


Fig. 11. Energy Band diagram of InAs/InGaAs DWELL sample B from Simulation.

Table 6

Representation of the different energy levels measured and calculated from experimental and simulation results, respectively.

Transition	Sample A		Sample B		Sample C	
	PL & PLE (eV)	Simulated energy (eV)	PL & PLE (eV)	Simulated energy (eV)	PL & PLE (eV)	Simulated energy (eV)
E_0-h_0	1.0857	1.08653	1.0616	1.06332	1.086	1.08812
E_1-h_1	1.1569	1.156	1.1307	1.1346	1.173	1.1912
E_2-h_2	1.229	1.2312	1.198	1.1929	1.259	1.281
Wetting layer	1.41–1.45		1.37–1.40		1.44–1.48	
Quasi-bound states	1.45–1.51		1.41–1.47		1.48–1.51	

of 6 nm and beyond this thickness the dot sublimation process occurs along with lateral size increment.

3.4. Simulation for calculating indium concentration in Qwell

Formation of quantum well with increasing capping thickness was confirm using various available optical and structural

characterization. In this section, a reverse approach with known PL energy peak for claimed Qwell structure is simulated to roughly calculate the average indium concentration in GaAs/ $In_xGa_{1-x}As$ /GaAs Qwell. In second part, the lateral and vertical size dependence of quantum is simulated and plotted. Confinement is affected by change in vertical dimension rather than that in lateral dimension. If we assume the formed Qwell has ground state peak near the first

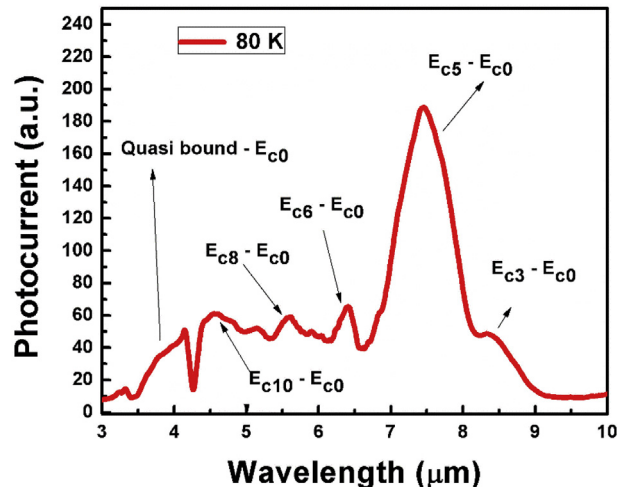
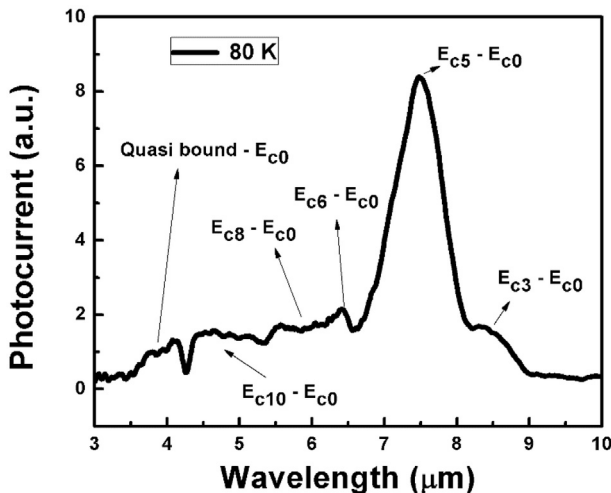


Fig. 12. Comparison of Spectral response with the theoretical model for Sample A.

Fig. 13. Comparison of Spectral response with the theoretical model for Sample B.

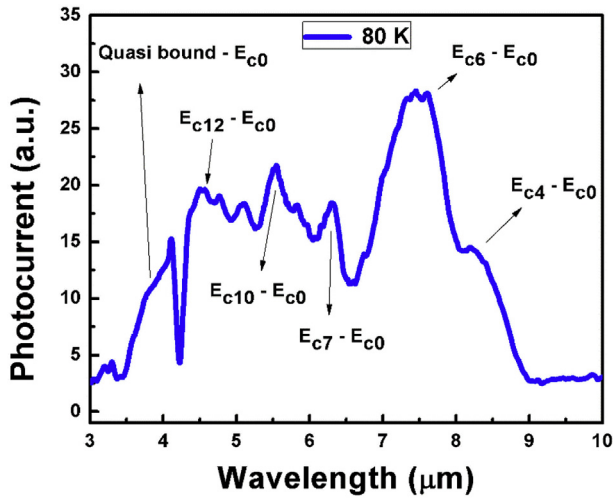


Fig. 14. Comparison of Spectral response with the theoretical model for Sample C.

excited state peak obtained from PL spectra shown in Fig. 2.a. The ternary alloy thickness was considered as 10 nm and the ground

state peak at 1085 nm. The average indium concentration inside the Qwell structure was found to be 0.305 which matches with the predicted value from People-Bean relation.

The wave function solution till the n states can be calculated and the potential profile of the InGaAs well can be obtained using proposed simulation. Transition energies corresponding to three excited states were 1.134, 1.262 and 1.419 eV. These energy levels are on par with PLE results in Fig. 5(b).

3.5. Vertical and lateral size dependence on energy spacing in QDs

As we have observed, the energy spacing is primarily dependent on vertical height. In this section, we are simulating a QD and tabulating the first four energy levels by keeping one dimension constant and varying the other. Initiating parameter for dot simulation is assumed from TEM images obtained for sample B. In the first case, a_1 & a_2 values are assumed to be same as mention in TEM images of sample B while the height (h) of quantum dot is varied from 2.5 to 4.5 nm in steps of 0.5 nm each (Fig. 15). In second case, height and top side length (a_1) are kept constant and lateral spacing (a_2) is varied. Similarly, a_1 can also be varied but the changes in energy level are insignificant. Hence the following simulation was performed in order to highlight the importance of vertical growth

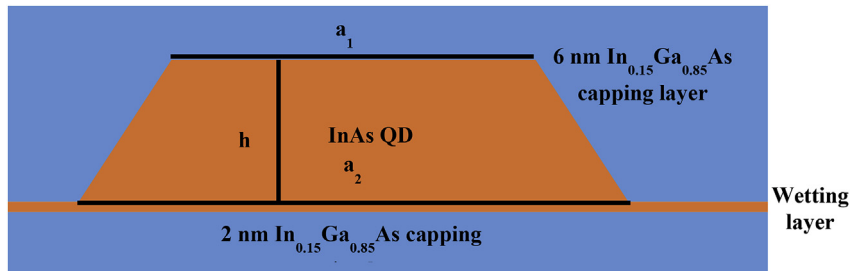


Fig. 15. Simulated quantum dot dimension.

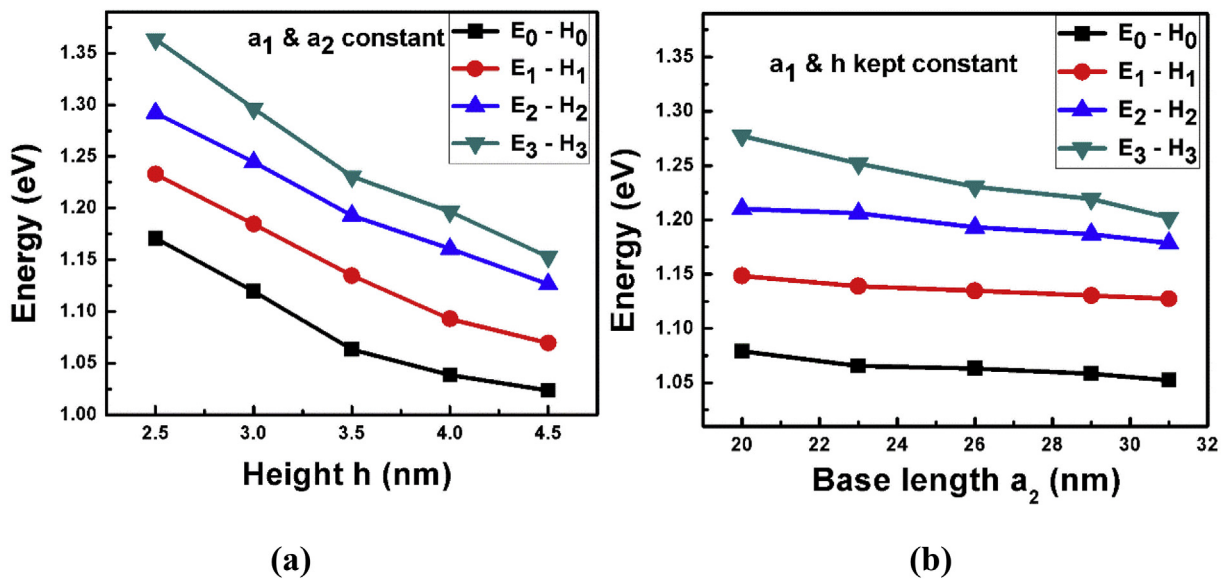


Fig. 16. Simulated energy levels (a) Varying QDs height (h) (b) Varying lateral length (a_2).

over lateral spreading through energy separation.

The calculated energy levels with varying height of QD is plotted in Fig. 16(a). The energy level spacing gradually increases as the thickness of the dot is reduced. Above 4.5 nm there is no significant change in ground state energy levels whereas the higher energy levels comes closer and closer thus increasing the electronics coupling in the structure. Varying lateral dimensions has insignificant effect on energy levels illustrated in Fig. 16(b). The QD confinement is essentially dependent on vertical growth rather than lateral stretching. After a certain height, the higher energy states are affected i.e. decrease in inter sub-band energy levels of higher states. This simulation shows that the energy states are dependent on the vertical dimension rather than horizontal dimension. Similarly, if we change the shape of QD to hemispherical, pyramidal or conical geometry the energy states shows a variation of $\pm 3\%$ as compared to truncated pyramid.

4. Conclusion

In conclusion, we report that sample B (6 nm strain reducing layer of $\text{In}_{0.15}\text{Ga}_{0.85}\text{As}$) is an optimized configuration for achieving highest optical, structural and infrared detector characteristics. Sample B exhibited nearly threefold increase in low temperature PL intensity as compared to other samples. Increasing capping thickness above 6 nm resulted in dot sublimation and formation of undesirable quantum well having non-linear indium concentration confirmed using various characterization techniques. According to TRPL results, longer excited carrier lifetime was achieved in sample B. Minimum dark current density with improved figure of merits was achieved in infrared detector fabricated using sample B. The proposed theoretical model is on par with the experimental results for various dot-in-a-well detector structures. The energy levels calculated using the model matches with experimental peaks obtained in PL and PLE spectroscopy. The model specifically points out particular transitions observed in spectral response from all the detector samples. Theoretically, the effective indium concentration in Qwell formed was calculated using reverse approach and the observed value was around 30%.

Acknowledgement

JP would like to thank CSIR (India) for fellowship. We thank DST (India) for financial grants DST-TM-SERIFR-117. The authors would also like to acknowledge DST Nanomission and National Center of Excellence in Technology for Internal Security (NCETIS). The authors acknowledge the financial support provided by the Department of Science and Technology, India, and partial support from IIT Bombay Nano Fabrication facility (IITBNF), Riber, of France.

References

- [1] H. Ghadi, S. Sengupta, S. Shetty, A. Manohar, and S. Chakrabarti, N. Pendyala, S. Prajapati and A. Kumar, "Comparison of three design architectures for quantum dot infrared photodetectors: InGaAs-capped dots, dots-in-a-well, and submonolayer quantum dots", *IEEE Trans. Nanotechnol.*, Vol. 14, No.4, pp.603–607.
- [2] S.J. Lee, J.C. Park, J.O. Kim, S.K. Noh, J.W. Choe, Effects of a cap layer on the confined sublevels in near-surface InAs/GaAs quantum dots, *J. Kor. Phys. Soc.* 46 (2005) 985.
- [3] E. Ahn, Y.S. Lee, J. Kim, E. Yoon, Y.D. Kim, In-situ monitoring of InAs/GaAs QDs by using spectral reflectance, *J. Kor. Phys. Soc.* 49 (2006) 947.
- [4] A. Madukar, Q. Xie, P. Chen, A. Konkar, InAs island-induced-strain driven adatom migration during GaAs overlayer growth, *Appl. Phys. Lett.* 64 (1994) 2727.
- [5] S.I. Jung, H.Y. Yeo, I. Yun, J.Y. Leem, S.M. Cho, J.S. Kim, J.I. Lee, High potential barrier effects on self-assembled InAs quantum dots, *J. Kor. Phys. Soc.* 50 (2007) 767–770.
- [6] S. Krishna, Quantum dots-in-a-well infrared photodetectors, *J. Phys. D* 38 (2005) 2147.
- [7] S. Sengupta, J.O. Kim, A.V. Barve, S. Adhikary, Y.D. Sharma, Sub-monolayer quantum dots in confinement enhanced dots-in-a-well heterostructure, *Appl. Phys. Lett.* 100 (2012) 191111.
- [8] Höglund, C. Asplund, Q. Wang, S. Almqvist, H. Malm, E. Petrini, J.Y. Andersson, P.O. Holtz, H. Pettersson, Origin of photocurrent in lateral quantum dots-in-a-well infrared photodetectors, *Appl. Phys. Lett.* 88 (2006) 213510.
- [9] R. Nedzinskas, B. Čechavičius, A. Rimkus, J. Kavaliauskas, G. Valušis, L.H. Li, E.H. Linfield, Optical features of InAs quantum dots-in-a-well structure, *Lithuanian J. Phys.* 54 (No. 1) (2014) 54–57.
- [10] K. Nishi, H. Saito, S. Sugou, J.-S. Lee, A narrow photoluminescence linewidth of 21 meV at 1.35 μm from strain-reduced InAs quantum dots covered by $\text{In}_{0.2}\text{Ga}_{0.8}\text{As}$ grown on GaAs substrates, *Appl. Phys. Lett.* 74 (1999) 1111.
- [11] H.Y. Liu, X.D. Wang, J. Wu, B. Xu, Y.Q. Wei, W.H. Jiang, D. Ding, X.L. Ye, F. Lin, J.F. Zhang, J.B. Liang, Z.G. Wang, Structural and optical properties of self-assembled InAs/GaAs quantum dots covered by $\text{In}_x\text{Ga}_{1-x}\text{As}$ ($0 \leq x \leq 0.3$), *J. Appl. Phys.* 88 (2000) 3392.
- [12] T. Tatebayashi, M. Nishioka, Y. Arakawa, Over 1.5 μm light emission from InAs quantum dots embedded in InGaAs strain-reducing layer grown by metal-organic chemical vapor deposition, *Appl. Phys. Lett.* 78 (2001) 3469.
- [13] H.Y. Liu, M. Hopkinson, C.N. Harrison, M.J. Steer, R. Frith, I.R. Sellers, D.J. Mowbray, M.S. Skolnick, Optimizing the growth of 1.3 μm InAs/InGaAs dots-in-a-well structure, *J. Appl. Phys.* 93 (2003) 2931.
- [14] J.X. Chen, U. Oesterle, A. Fiore, R.P. Stanley, M. Illegems, T. Todaro, Matrix effects on the structural and optical properties of InAs quantum dots, *Appl. Phys. Lett.* 79 (2001) 3681.
- [15] L. Seravalli, M. Minelli, P. Frigeri, P. Allegri, V. Avanzini, S. Franchi, The effect of strain on tuning of light emission energy of InAs/InGaAs quantum-dot nanostructures, *Appl. Phys. Lett.* 82 (2003) 2341.
- [16] J. Kim, C.J. Yang, U. Sim, E. Yoon, Y. Lee, W.J. Choi, Effects of the well layer on the emission wavelength of InAs/InGaAs dot-in-a-well structure, *J. Kor. Phys. Soc.* 52 (February 2008) S34–S37.
- [17] Hemant Ghadi, Navneet Sehara, Punam Murkute, Subhananda Chakrabarti, Minimization of material inter-diffusion for thermally stable quaternary-capped InAs quantum dot via strain modification, *Superlattice. Microst.* 105 (May 2017) 117–131.
- [18] Hemant Ghadi, S. Chakrabarti "reportHigh Performance Strain Coupled InAs/GaAs Quantum Dot-based Infrared Photodetectors and Demonstration of Focal Panel Arrays", Ph.d. Thesis, 2011-16, IIT Bombay.
- [19] M. Srujan, K. Ghosh, S. Sengupta, S. Chakrabarti, Presentation and experimental validation of a model for the effect of thermal annealing on the photoluminescence of self-assembled InAs/GaAs quantum dots, *J. Appl. Phys.* 107 (June 2010) 123107.
- [20] Z. Zaaboub, F. Hassen, M. Naffouti, H. Maaref, Temperature effect on the electronic transfer mechanism between InAs/GaAs quantum dots by the mean of time resolved photoluminescence spectroscopy, *J. Mater. Sci. Eng. Adv. Technol.* 14 (1) (2016) 1–17.
- [21] Minh Tan Man, Hong Seok Lee, Discrete states and carrier-phonon scattering in quantum dot population dynamics, *Sci. Rep.* 5 (2015), Article 8267.
- [22] Bouzaiene, B. ilahi, S. faxi1, F. hassen1, H. maaref1, O. marty2, J. dazor, Tuning vertically stacked InAs/GaAs quantum dot properties under spacer thickness effects for 1.3 μm emission, *Appl. Phys. A* 79 (2004) 587–591.
- [23] T. Switański, U. Woggon, Carrier dynamics in InAs/GaAs submonolayer stacks coupled to Stranski-Krastanov quantum dots, *Phys. Rev. B* 88 (2013), 035314.
- [24] F. Pulizzi, A.J. Kent, A. Patané, L. Eaves, M. Henini, Time-resolved photoluminescence of InAs quantum dots in a GaAs quantum well, *Appl. Phys. Lett.* 84 (2004) 3046.
- [25] L. Kong, Z.C. Feng, Z. Wu, W. Lu, Temperature dependent and time-resolved photoluminescence studies of InAs self-assembled quantum dots with InGaAs strain reducing layer structure, *J. Appl. Phys.* 106 (2009), 013512.
- [26] L. Ya. Karachinsky, S. Pellegrini, G.S. Buller, A.S. Shkolnik, N. Yu. Gordeev, V.P. Evtikhiev, V.B. Novikov, Time-resolved photoluminescence measurements of InAs self-assembled quantum dots grown on misoriented substrates, *Appl. Phys. Lett.* 84 (2004) 7.
- [27] J. Patwari, H. Ghadi, S. Sardar, J. Singhal, B. Tongbram, S. Shyamal, C. Bhattacharya, S. Chakrabarti, S. Pal, "Photo-induced electronic properties in single quantum well system: effect of excitonic lifetime", *Mater. Res. Express* 4 (2017) 016301.
- [28] R. People, J.C. Bean, Calculation of critical layer thickness versus lattice mismatch for $\text{Ge}_{x}\text{Si}_{1-x}/\text{Si}$ strained layer heterostructures, *Appl. Phys. Lett.* 47 (1985) 322.
- [29] Seyoum Wolde, Yan-Feng Lao, A.G. Unil Perera, Y.H. Zhang, T.M. Wang, J.O. Kim, Ted Schuler-Sandy, Zhao-Bing Tian, S. Krishna, Noise, gain, and capture probability of p-type InAs-GaAs quantum-dot and quantum dot-in-well infrared photodetectors, *J. Appl. Phys.* 121 (2017) 244501.